14TH CANADIAN MASONRY SYMPOSIUM
MONTREAL, CANADA
MAY 16TH – MAY 20TH, 2021

EXAMINING THE MODE OF FAILURE OF SLENDER CONCRETE BLOCK WALLS

Ahmed, Ahmed[1]; Iskander, George[2]; Bogoslavov, Mihailo[3]; Isfeld, Andrea[4] and Shrive, Nigel[5]

ABSTRACT

Slender concrete masonry walls can fail through compression, flexure or buckling. Previous finite element modelling showed the governing mode of failure of axially loaded walls depends on both slenderness and load eccentricity. However, exterior walls will be subjected to lateral as well as axial loads. Therefore, the effect of lateral pressure on the failure mode of unreinforced, ungrouted slender concrete masonry walls was investigated. Finite element models of walls with and without lateral loads representing average Canadian wind pressures were compared to assess the influence of lateral load on wall capacity and failure mode. Such models were analyzed across a broad range of axial load eccentricities and slenderness ratios. The effect of the distribution of the lateral pressure (triangular vs. rectangular) was also investigated. Models loaded with lateral pressures corresponding to maximum Canadian wind pressures were also analyzed but over a smaller range of axial load eccentricities and slenderness ratios. Certain walls, which the Canadian Standard for the Design of Masonry Structures, CSA S304-14 deems slender, failed in compression when loaded at a low axial load eccentricity, despite the applied lateral pressure. Hence, it is proposed that CSA S304 should classify slender walls by failure mode which would greatly reduce the current inaccuracy in the design of slender walls loaded at low axial load eccentricities.

KEYWORDS: *slender walls, out-of-plane bending, mode of failure*

[1] PhD student, Department of Civil Engineering, University of Calgary, 2500 University Dr NW, Calgary, AB, Canada, ahmed.ahmed1@ucalgary.ca
[2] PhD student, Department of Civil Engineering, University of Calgary, 2500 University Dr NW, Calgary, AB, Canada, george.iskander@ucalgary.ca
[3] MSc student, Department of Civil Engineering, University of Calgary, 2500 University Dr NW, Calgary, AB, Canada, mihailo.bogoslavo1@ucalgary.ca
[4] Research Associate, Department of Civil Engineering, Newcastle University, University Dr, Callaghan NSW 2308, Australia, andrea.isfeld@newcastle.edu.au
[5] Professor, Department of Civil Engineering, University of Calgary, 2500 University Dr NW, Calgary, AB, Canada, ngshrive@ucalgary.ca

INTRODUCTION

The Canadian Standard for the Design of Masonry Structures, CSA S304-14, [1] requires masonry walls to be designed accounting for secondary moment effects when the slenderness ratio (defined as the ratio of effective height to wall thickness, *kh/t*) exceeds the value of 10-3.5(e_1/e_2), with 'e_1' and 'e_2' representing the top and bottom end moment eccentricities respectively. When the slenderness ratio exceeds a value of 30, the allowable axial load applied to the wall is limited to 10% of its axial load capacity, while at ratios below 30 the allowable axial load is limited to 80% of the axial load capacity.

The provisions governing the design of slender masonry walls in CSA S304-14, [1] have been shown to lead to overly conservative design. Müller et al. [2] demonstrated the extent to which slender concrete block walls were being overdesigned. The authors noted that slender walls were particularly overdesigned at low axial load eccentricities. This observation was hypothesized to be a result of CSA S304-14's under-estimation of the effective flexural stiffness (EI_{eff}), and deviation of experimentally established wall fixed ends from theoretical fixed behaviour. Using the results of the extensive testing program of Hatzinikolas et al. [3], Bogoslavov & Shrive [4] compared the experimental response of walls deemed standard by CSA S304-14 to their capacities in accordance with CSA S304-14. It was indeed found that EI_{eff} was under-estimated by CSA S304-14, resulting in over-estimations of deflections and secondary moments (and thus, over-designed walls) at low axial load eccentricities. Further, it was observed that slender walls loaded at low axial load eccentricity by Hatzinikolas et al. [3] failed by vertical splitting (indicating material failure), rather than the out-of-plane failure typical of slender walls. These experiments suggest that CSA S304-14 mischaracterizes the failure mode of slender walls at low eccentricities, resulting in significant underestimation of capacity.

Isfeld et al. [5] modelled unreinforced concrete block walls of varying slenderness ratios and axial load eccentricities and categorized them by failure mode based on their height to thickness ratio and axial load eccentricity. In the reported results, walls were distinguished as failing with all bed joints fully closed, bed joints with partial contact, or some bed joints fully open. Notably, walls loaded with axial load eccentricities of t/6 or less (where 't' represents the wall thickness) failed with bed joints fully closed, even at height to thickness ratios over 30. Isfeld et al. [5] thus showed that slenderness ratio alone was not enough to determine the failure mode of a wall. More accurate design could be achieved if the Standard differentiated walls according to their expected failure modes and accordingly prescribed design procedures.

Implementation of a failure-mode based design procedure for slender walls requires determination of the influence of lateral load on the mode of failure. Hence, the influence of lateral load on the failure mode of slender, unreinforced, ungrouted concrete masonry walls was investigated. For the purpose of this study, lateral loads were determined via the National Building Code of Canada [6]. The behaviour of slender masonry walls loaded at a low axial load eccentricity is of a particular interest, as these walls have been shown through modelling (by Isfeld et al. [5]) and testing (by Hatzinikolas et al. [3]) to fail in compression when no lateral load had been applied.

NUMERICAL MODEL DESCRIPTION

Modelling Technique

Finite element analysis was performed using Abaqus. The 3D detailed micro-modelling approach was used, in which units and mortar are modelled separately and interaction properties between them are assigned. While Lourenco [7] introduced this approach for modelling brickwork, Isfeld et al. [8] used it to model block masonry walls and found good agreement with experimental results.

Test Array

Forty-seven ungrouted, unreinforced, face-shell bedded, concrete block walls were modelled; all walls were three blocks (1200 mm) wide. The models included a reference model as well as three groups: a full parametric study, a smaller parametric study, and model verification.

The main parametric study investigating the effect of average Canadian wind pressures on wall axial capacity consisted of three sets of 12 walls, as described in Table 1. Walls varied in slenderness ratio, axial eccentricity, and out-of-plane loading. Each unique combination of variable values was modelled once for a total of 36 walls.

Table 1: Main Parametric Study with Average Wind Pressure

Variable Type	Values Considered
Slenderness ratio, h/t	10, 20, 30, 40
Axial Load Eccentricity, e	0, t/10, t/6
Out-of-Plane Load	None, Average Rectangular, Average Triangular
Boundary Conditions	Fixed-pinned

A smaller parametric study was conducted to investigate the effect of maximum Canadian wind pressures on axial capacity. The variables considered are described in Table 2. Each unique combination of values was once again modelled, for a total of 8 walls.

Table 2: Smaller Parametric Study with Maximum Wind Pressure

Variable Type	Values Considered
Slenderness ratio, h/t	10, 40
Axial Load Eccentricity, e	0, t/6
Out-of-Plane Load	None, Max. Rectangular, Max. Triangular
Boundary Conditions	Fixed-pinned

Two additional walls were modelled to validate the modelling by comparing their load-displacement behaviour with experimental data from walls with pinned-pinned boundary conditions tested by Hatzinikolas et al. [9]. Finally, a five-unit high wall with no out-of-plane

pressure and concentric axial load was modelled. This model provided a representative value for pure axial capacity (referred to as P_o).

Part Geometry

The walls were assembled using standard hollow concrete masonry units (CMUs) of dimensions 390 x 190 x 190 mm. The block geometry accurately captures the taper of the cores in a standard CMU. All mortar joints were 10 mm thick. 63.5 mm thick steel bearing plates were placed at the top and bottom of the wall to distribute applied axial loads. A 60 mm diameter steel roller, through which axial load was applied, was placed on the top bearing plate. A typical assembled wall is shown in Figure 1a), with the roller used to apply axial load and the tapered blocks used to compose the model being shown in Figures 1b) and c), respectively.

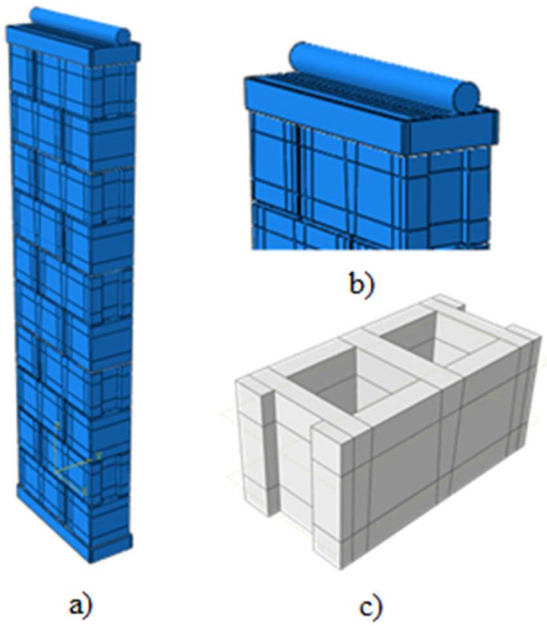

Figure 1: Wall Assembly Figures: a) Overall Assembly, b) Roller Used for Axial Load Application, c) Tapered Blocks Used in Wall Assembly.

Material Properties

Material models were reflective of typical blocks and mortar and included elastic as well as plastic material behaviour. Simplified stress-strain curves in tension and compression, remaining linear until peak load, were used to reduce computational effort. The Concrete Damage Plasticity model was used to capture the plasticity behaviour of both materials, with damage parameters matching those used by Isfeld et al. [5] to permit comparison between the results of both sets of modelling.

The material properties used for blocks and mortar in this study are listed in Table 1. Material property set ‘A’ was based on average values reported from the Hatzinikolas et al. [9] testing program. Material property set ‘A’ was used only in the 2 walls modelled to compare with the

Hatzinikolas et al. [9] experimental data. Material property 'B' matched the properties used by Isfeld et al. [1] to allow for meaningful comparison of the two modelling techniques. All other walls were modelled using property set 'B'. Poisson's ratio was taken as 0.2 for both material property sets.

Table 3: Material Property Sets

Material Property Set	Block E (MPa)	Block f'_c (MPa)	Block f'_t (MPa)	Mortar E (MPa)	Mortar f'_c (MPa)	Mortar f'_t (MPa)
A	9300	13.5	1.35	4800	11	1.1
B	11950	18.6	1.86	4500	10.75	1.075

As the steel bearing plates and roller were not expected to approach yield, steel was only defined with elastic material properties – typical values (E = 200,000 MPa, $\nu = 0.3$) were used.

Element Type and Mesh Refinement

Eight-node 3D "brick" elements (C3D8) were used to model both blocks and mortar. Mesh sensitivity analysis was performed revealing that a global mesh size of 20 mm within the blocks and 15 x 15 x 5 mm elements within the mortar joints achieved mesh independency with reasonable solving time. Reducing the element thickness to 5 mm in the mortar joint allowed for improved refinement of the stress distribution through the joint thickness while avoiding distorted element geometry. A meshed block is shown in Figure 2a) and mortar mesh in Figure 2b).

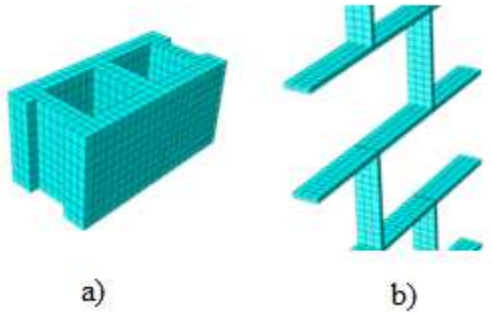

Figure 2: Typical Meshes: a) Blocks, b) Mortar.

Interaction Properties

Contact interaction properties were used to model the normal and tangential behaviours of both the head and bed joints. Normal behaviour was defined within Abaqus using "hard contact" and default constraint enforcement. Tangential behaviour was defined using the penalty friction formulation included in Abaqus, with an isotropic frictional coefficient of 0.7. Cohesive strength values of 0.5 and 0.25 MPa were taken to represent the cohesive normal and tangential damage initiation stresses; traction-separation behaviour was defined via uncoupled stiffness coefficients,

with a stiffness of 2650 MPa in the normal direction and 1300 MPa in the tangential directions. Bilinear damping was also defined in the interaction to ensure convergence.

Boundary Condition Implementation

To provide a pinned-fixed boundary condition for the wall, the roller's out-of-plane displacements were restrained and the lower bearing plate was fixed. To reduce computational demand, half of the wall width was explicitly modelled and symmetric boundary conditions were applied along the wall axis. Pinned-pinned boundary conditions were obtained by restraining the roller's out-of-plane displacements and pinning the centreline of the lower bearing plate in the direction of the wall's width.

Load Determination and Application

All loads were applied over the course of a single static step. The full magnitude of the out-of-plane loading was applied at the beginning of the static step; out-of-plane loads were either rectangular or triangular distributed loads. Axial loads were ramped over the duration of the step. The system response was determined assuming quasi-static behaviour.

The "Static Procedure" as defined by 4.1.7.3, NBCC 2015 [6], was used to determine average and maximum Canadian wind pressures. Walls were assumed to be in open terrain, main structural elements on the windward face, and in structures of normal importance. Hourly wind pressure values with a probability of exceedance of 1 in 50 years were used in the calculations. The average of all 1/50 hourly wind pressures available in Table C-2, NBCC 2015, was used in conjunction with the aforementioned assumptions to determine the average Canadian rectangular wind pressure – this value was found to be 0.45 kPa. To compare the effects of pressure distribution (triangular vs. rectangular) on axial capacity, a triangular pressure distribution, linearly increasing from zero at the base until the top of the wall, with an equal resultant force was also used. The triangular pressure distribution corresponding to average Canadian wind pressures thus had a peak pressure of 0.90 kPa at the top of the wall.

Maximum Canadian wind pressures were determined similarly, but the maximum 1/50 hourly wind pressure in Table C-2, NBCC 2015 was used in place of the average value. This yielded a magnitude of 1.15 kPa for the rectangular case and a peak value of 2.30 kPa for the triangular case.

Axial loads were applied via vertical displacements through the roller. Eccentric axial load was applied by placing the roller on the top bearing plate at the required eccentricity.

RESULTS

Validation Against the Hatzinikolas et al. Testing Program

To assess the accuracy of the developed finite element model, two walls (named T1 & T2) closely resembling specimens from the Hatzinikolas et al. [4] testing program were modelled. These walls were highly similar in geometry, with identical boundary conditions and load application (i.e. no out-of-plane loading) compared to the Hatzinikolas et al. specimens. Material property set A was

used to provide a reasonable match to the material properties listed by Hatzinikolas et al. for their specimens. The two walls modelled represent a broad range of slenderness and axial load eccentricity. The ultimate compressive loads from the finite element model are compared to the experimental failure loads from the comparable specimens in the Hatzinikolas et al. tests in Table 4; as may be seen the results are in reasonably close agreement.

Table 4: Verification of FE Model against Hatzinikolas et al. [4] results.

Model	$(h/t)_{model}$	e_{model} (mm)	P_{model} (kN)	Comparable Specimen	$(h/t)_{exp.}$	$e_{exp.}$ (mm)	P_{exp} (kN)	P_{model}/P_{exp}
T1	5.24	63.33 (t/3)	864	Short Wall 5	5.15	64.5 (t/3)	708	1.22
T2	20.95	31.67 (t/6)	787	Plain Wall G1	17.97	32.3 (t/6)	714	1.10

Validation Against Isfeld et al. Models

Further validation was performed by comparing the results obtained with the finite element results presented by Isfeld et al. [1] for unreinforced masonry walls with pinned-fixed boundary conditions. The results are shown in Figure 3 for the case of e = t/10; the general trend of the results is similar for all eccentricities considered in this study. Axial capacities are normalized to the value P_o, which is the axial capacity via the new model for a 5-unit high wall under axial compression with no out-of-plane load.

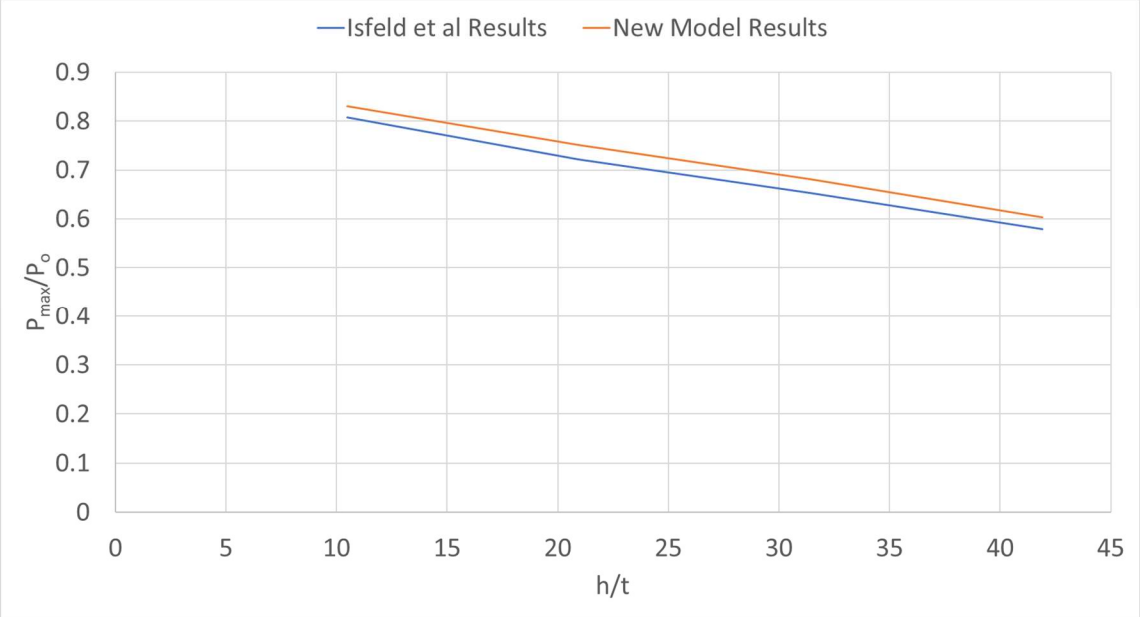

Figure 3: Comparison of Results from New Model to Results from Isfeld et al. [1]

The general trend of the new model strongly agrees with the Isfeld et al. [1] results. The slight increase in strength of the new model can be attributed to the inclusion of unit-mortar interface

cohesive behaviour in the new model, which allows the wall to resist flexural deformation to a higher degree.

Influence of Average Canadian Wind Pressures on Wall Capacity

The axial capacities of walls subjected to out-of-plane (OOP) loads corresponding to average Canadian wind pressures compared to walls with no OOP loads are shown in Figures 4a) through 4c). Results were plotted for eccentricity (e) values of 0, t/10, and t/6. Maximum loads are again normalized to the value P_o. Only in the case of e = 0 at a h/t of 40 did the average wind pressures affect axial capacity to a potentially meaningful degree; the reduction in this case being about 7%, as may be seen in Figure 4a).

Further, while a triangular OOP pressure distribution reduced axial capacity more than the rectangular OOP distribution, the difference was minimal across the range of eccentricities and h/t ratios investigated.

To investigate the effect of OOP loading on the failure mode, the failure modes for walls with average Canadian OOP wind loads were compared to the failure modes reported by Isfeld et al. [1] for identical walls without OOP load. Among all walls tested, identical observations were found for rectangular and triangular OOP pressure distributions. OOP load changed the failure mode from the Isfeld et al. findings in only one case – at e = t/6 and h/t = 40. Horizontal mortar joints in this case were partially in contact at failure, indicating flexural failure instead of compressive failure. Joint status at failure for models with and without average Canadian OOP wind loading is reported in Table 3.

Table 3: Joint Status at Failure for Walls With and Without Average OOP Wind Load

h/t	Joint Status at Failure					
	e = 0		e = t/10		e = t/6	
	No OOP Load	OOP Load	No OOP Load	OOP Load	No OOP Load	OOP Load
10	Closed	Closed	Closed	Closed	Closed	Closed
20	Closed	Closed	Closed	Closed	Closed	Closed
30	Closed	Closed	Closed	Closed	Closed	Closed
40	Closed	Closed	Closed	Closed	Closed	Partial Contact

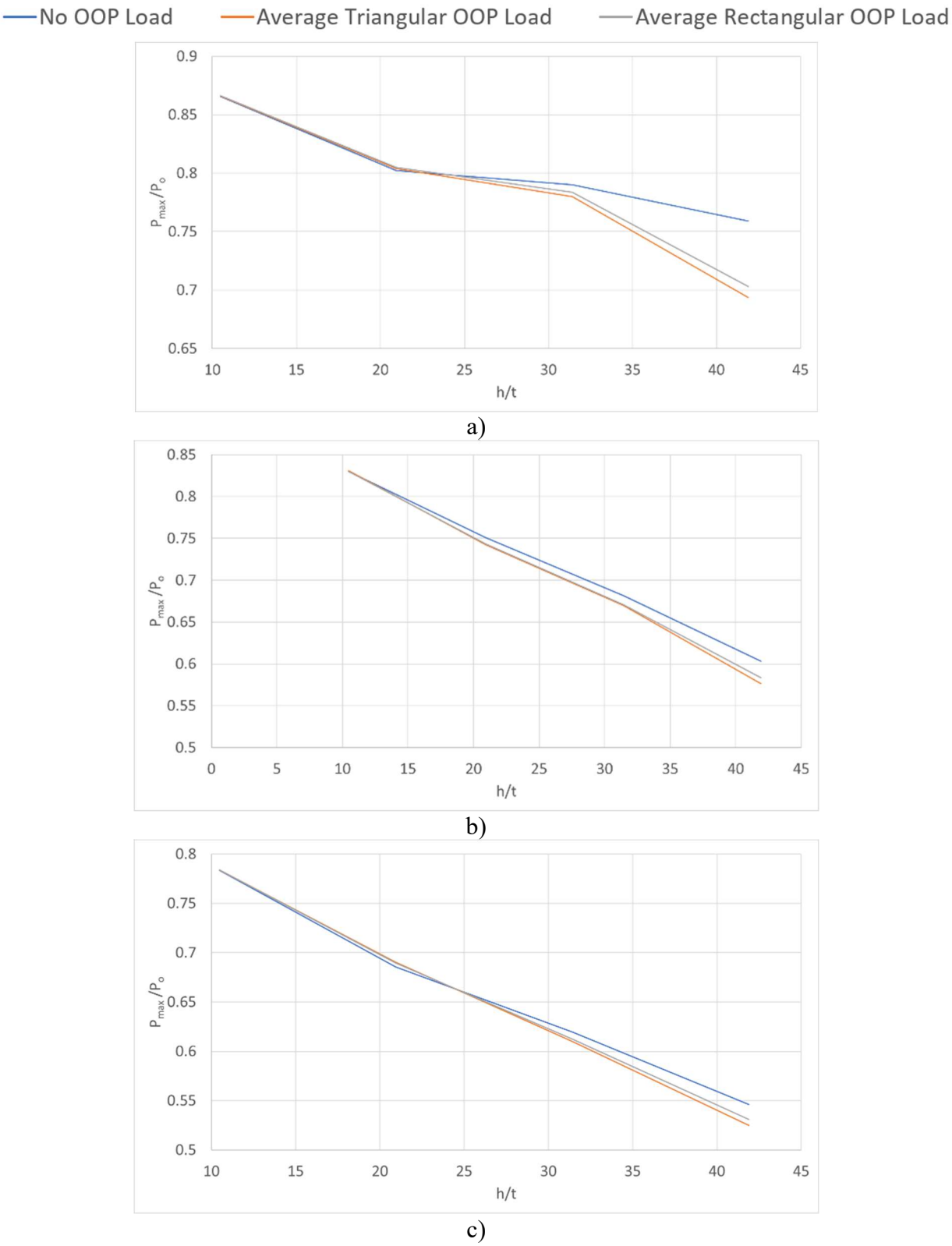

Figure 4: Variation of Wall Axial Capacity Under Average Canadian OOP Wind Loading with h/t: a) e = 0, b) e = t/10, c) e = t/6.

Influence of Maximum Canadian Wind Pressures on Axial Capacity

The axial capacities of walls with no OOP load are compared to those subjected to triangular and rectangular OOP pressures corresponding to maximum Canadian wind effects in Figures 5 a), b) and c).

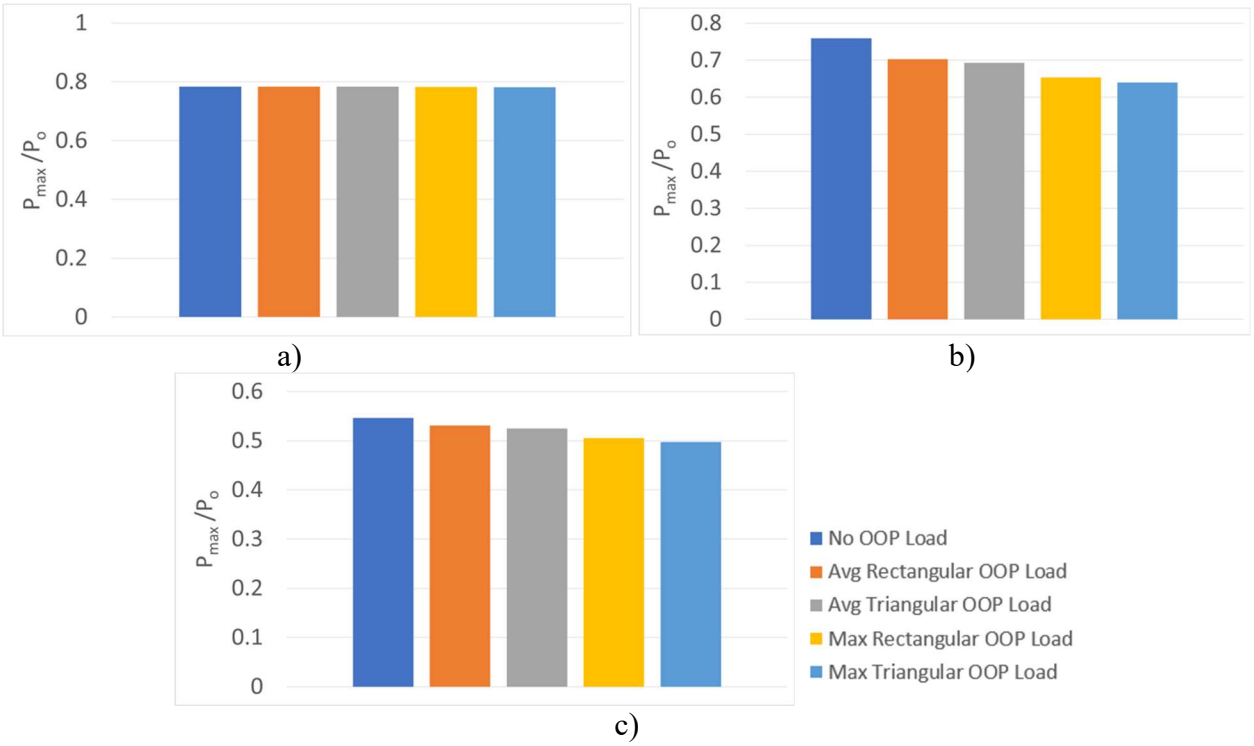

Figure 5: Variation of Wall Axial Capacity Under Maximum & Average Canadian OOP Wind Loads: a) h/t = 10, e = t/6; b) h/t = 40, e = 0; c) h/t = 40, e = t/6.

Maximum wind loads were still insufficient to impact the results meaningfully at h/t = 10 for both e = 0 and e = t/6. At h/t = 40, the reduction in capacity due to maximum OOP loading is roughly double the reduction observed due to average OOP load. This reduction was not exactly equal to the increase in the load – the maximum wind pressure applied was 2.55x the average value.

CONCLUSIONS

The finite element models demonstrate that even the addition of lateral loads corresponding to maximum Canadian wind pressures did not cause slender walls at low eccentricities to exhibit signs of flexural failure. The reduction in wall axial capacity of walls due to lateral load increased with slenderness, although even at the highest modelled slenderness ratio (h/t=40), the reduction did not exceed 10%. Further, inclusion of average Canadian wind pressures was sufficient to change the failure mode only in the most extreme of the examined cases (h/t = 40, e/t = t/6). If such walls were being designed today using CSA S304-14, [1] the walls would have been designed to account for secondary moment effects, and thus significantly overdesigned. It is therefore recommended that CSA S304 should consider the nature and the magnitude of the loading on the wall in addition to its slenderness ratio in prescribing the required design procedure.

The necessary next step would be to model walls with even higher slenderness ratios and axial load eccentricities to capture the dependence of failure mode on slenderness ratio, lateral loading and eccentricity more completely. As unreinforced slender walls are uncommon in practice, models must also be made for reinforced and grouted slender walls. An extensive testing program must also be undertaken to verify the results of the modelling. Such work will eventually lead to the development of an improved method for the design of walls without the sudden drop in allowable axial load at kh/t = 30 as currently specified by CSA S304-14.

The calculation of effective flexural stiffness, EI_{eff}, as detailed in the Standard was not considered in the current study. The effective stiffness is used to estimate the reduction in stiffness of a wall as cracking occurs and is necessary for the calculation of the secondary moment. Improving the accuracy of the effective flexural stiffness term will therefore significantly benefit the accuracy of slender wall provisions when out-of-plane failure is expected. The effect of top and bottom wall fixity will also be examined in future work.

ACKNOWLEDGEMENTS

We gratefully acknowledge the support of the Natural Sciences and Engineering Research Council of Canada, the Canadian Concrete Masonry Producers Association and the University of Calgary. Support from Compute Canada is also gratefully acknowledged.

REFERENCES

[1] Canadian Standards Association. (2014). *S304.1-14 Design of Masonry Structures*, CSA Group, Mississauga, ON, Canada.

[2] Müller, A.L., Isfeld, A.C., Hagel, M., Shrive, N.G. (2017). "Review and Analysis of Capacity of Slender Concrete Masonry Walls". *Proc., 13th Canadian Masonry Symp*., Halifax, NS, Canada.

[3] Hatzinikolas, M., Longworth, J., Warwaruk, J. (1978). *Concrete Masonry Walls*, *Structures Report No. 70*, University of Alberta, Edmonton, AB, Canada.

[4] Bogoslavov, M. and Shrive, N.G. (2020). "The Influence of Effective Flexural Stiffness on Slender Masonry Wall Capacity". *Proc., 17th International Brick and Block Masonry Conference*, Krakow, Poland.

[5] Isfeld, A.C., Hagel, M., Shrive, N.G. (2019). "Finite Element Analysis of Hollow Concrete Block Masonry Walls". *Proc., 13th North American Masonry Conference*, Salt Lake City, Utah, USA.

[6] National Research Council of Canada. (2015). *National Building Code of Canada 2015,* Canadian Commission on Building and Fire Codes, Ottawa, ON, Canada.

[7] Lourenco, P.B. (2002). "Computations on Historic Masonry Structures", *Progress in Structural Engineering and Materials,* 4 (3), 301-319.

[8] Isfeld, A.C., Muller, A.L., Hagel, M, Shrive, N.G. (2020). "Testing and finite element modelling of concrete block masonry walls under axial and out-of-plane loading." *International Journal of Masonry Research and Innovation,* 6(1), 60-80.

[9] Hatzinikolas, M., Longworth, J., Warwaruk, J. (1978). *Experimental Data for Concrete Masonry Walls, Structural Engineering Report No.71*, University of Alberta, Edmonton, AB, Canada.